Supplementary File 1

Daniela Carrasco Guerrero[†1], Natalia Vidal Barraza[†2], Patricio Riquelme[3,4], María E. Castelló[5], Joseph Yuan-Mou Yang[6,7,8], Cecilia Hernández[9], Pamela Guevara[1*]

[1*]Electrical Engineering Department, Faculty of Engineering, Universidad de Concepción, Concepción, Chile.
[2]Faculty of Engineering, Universidad de Concepción, Concepción, Chile.
[3]Department of Medical Technology, Faculty of Medicine, Universidad de Chile, Santiago, Chile.
[4]Laboratory of Neuropsychology and Clinical Neurosciences, Faculty of Medicine, Universidad de Chile, Santiago, Chile.
[5]Desarrollo y Evolución Neural, Depto. Neurociencias Integrativas y Computacionales, Instituto de Investigaciones Biológicas Clemente Estable, Montevideo, Uruguay.
[6]Neuroscience Advanced Clinical Imaging Service (NACIS), Department of Neurosurgery, The Royal Children's Hospital, Melbourne, Australia.
[7]Neuroscience Research, Murdoch Children's Research Institute, Parkville, Melbourne, Australia.
[8]Department of Paediatrics, University of Melbourne, Parkville, Melbourne, Australia.
[9*]Computer Science Department, Faculty of Engineering, Universidad de Concepción, Concepción, Chile.
[†] These authors contributed equally to this work..

*Corresponding author(s). E-mail(s):
pamela.guevara@biomedica.udec.cl;
Contributing authors: daniela.carrasco@biomedica.udec.cl;
natalia.vidal@biomedica.udec.cl; pfriquelme@uchile.cl;
mcastello@iibce.edu.uy; joseph.yang4@rch.org.au;
cecihernandez@udec.cl;

1 List of connections

A detailed description of the white matter pathways included in the atlas is presented. For each connection, an anatomical description is defined based on its origin, termination, and its trajectory through the main cerebral structures. This provides the necessary neuroanatomical context to understand the functional role of the pathway.

For selected pathways, we specify the regions of interest derived from established literature and validated neuroanatomical protocols. To maintain consistency, any reference to figures from these external studies (e.g., anatomical demonstration, ROIs placements) follows the original numbering used in the cited source.

1.1 Cerebello-ponto-hypothalamic tract (CPH)

The CPH tract originates from the cerebellar hemisphere, coursing through the ipsilateral middle cerebellar hemisphere. The CPH tract then enters the pons, where it crosses to the contralateral pons through the transverse pontine fibers [1]. After crossing to the other side, the CPH tract then ascends in the pons into the midbrain, where it ascends at the junction of the cerebral peduncle/tegmentum of the midbrain. The CPH tract then projects into the posterior aspect of the cerebral peduncle and ascends alongside the temporopontine tract [1].

The CPH tract deviates laterally into the medial aspect of the parahippocampal gyrus (Fig. 3b) [1]. Within the medial margin of the parahippocampal gyrus, the CPH tract changes course and projects ventrally along the superior and lateral aspect of the optic tract (Figs. 3b, 4d) [1]. The CPH then projects more medially in relation to the optic tract distally (Fig. 4d) [1]. The CPH tract courses ventrally alongside the anterior arms of the fornix (Fig. 4c) [1]. Finally, the CPH terminates in the region of the anterior hypothalamic nuclei (arrow in Fig. 3a)[1] just posterior to the optic chiasm [1].

Fig 11 [2] shows the DTI images of seven cases showing the direct cerebello-hypothalamic pathways via SCP.

1.2 Cerebello-thalamo-cortical tract (CTC)

The cerebello-thalamo-cortical pathway connects the cerebellum with the cerebrum, passing through the superior cerebellar peduncle (SCP) and the contralateral thalamus [3]. The proximal segment of the cerebellothalamocortical tract is particularly vulnerable to surgical damage [4].

Fig. 4 [3] shows the streamlines of the CPC pathway (red) in a representative subject to demonstrate the whole extent of the CPC pathway and to consistently identify its different portions, e.g., fronto-ponto-cerebellar or temporo-ponto-cerebellar tracts. It is worth noting that areas reached by the majority of streamlines are the temporal and frontal lobes in the cerebrum, and the lateral Crus I-II and lobules VIIb/VIII in the cerebellum. Moreover, the CPC pathway does not enter the thalamus but instead runs just outside this area, passing correctly through the internal capsule [3].

Fig. 4 [5] also shows a 2D rendering of both cerebello-thalamo-cortical pathways from a representative subject. In particular, Fig. 4a shows the tracts colour-coded by direction in order to represent their anatomy, while Fig. 4b [5] shows the same tracts using a single colour per tract in order to distinguish left from right-side streamlines, highlighting their extensions into the cerebral and cerebellar cortices [5].

Figs. 2a and 2b [6] show, respectively, the mean cerebello-thalamo-cortical pathway reconstructed using ROIs placed on b0 and on TDI for both hemispheres in MNI space. Both seeding approaches resolved the decussation; however, ROIs identified on the TDI maps provided a better reconstruction capable of isolating those cerebellar pathways originating from the SCP and avoiding all other cerebellar contributors (Fig. 2c) [5]. By contrast, when using the ROIs defined on the b0 images the reconstructed

pathways erroneously included cerebellar tracts running from body districts to the cerebellum and passing through the SCP [6].

- ROIs

  Cerebello-thalamo-cortical pathways were reconstructed by combining the CSD algorithm with probabilistic tractography and by tracking the bundle passing through two regions of interest (ROIs): the SCP and the contralateral RN. These pathways were reconstructed by randomly seeding streamlines throughout the SCP seed ROI until 3,000 streamlines were reconstructed. To compare this with the conventional diffusion tensor model, cerebello-thalamo-cortical pathways were also reconstructed using a DTI-based streamline deterministic tractography by randomly seeding streamlines throughout the seed ROI defined by the SCP, and using the following parameters: step size = 0.1 mm, maximum angle between steps = 4.5°, FA $\geq$ 0.2, termination criteria: exit the brain or when the FA was $<$ 0.1; once again, a total of 3,000 streamlines were reconstructed. No contralateral target ROI was defined because with this approach tracts run only ipsilaterally [5].

  SCP and RN masks were placed using the high-resolution TDI images. The seed ROI was defined as a sphere with a 2 mm radius centred on the SCP in each cerebellar hemisphere and was identified in the coronal plane, as described by Calamante et al. [7], while the target ROI on the whole contralateral RN was recognized as a very hypointense region [5].

  When the ROI is placed in the region of the ventro-lateral thalamus, fiber trajectories decussate to the contralateral cerebellum and penetrate the medullary core of the cerebellum in the region of the deep cerebellar nuclei. Some fiber trajectories that emanate from the thalamic ROI towards the cerebellum cannot be traced to the cerebellum itself. Other fiber solutions identified by the thalamic ROI continue into the spinal cord, likely reflecting ascending spino-thalamic fiber systems [8].

The ROI placed in the red nucleus in Fig. 5b [8] results in a contingent of fibers that courses into the cerebellum, consistent with the known efferent pathway leading from the interpositus nucleus via red nucleus to thalamus. Other fiber solutions course towards the spinal cord. This may reflect fibers in the rubrospinal tract, but it is also possible that it reflects corticospinal fibers in the cerebral peduncles adjacent to the ROI in the red nucleus [8].

Fig. 1 [6] allows a qualitative comparison between seed/target ROIs (always defined on anatomical bases) on b0 images and those defined on TDI images. Fig 1b [6]shows a schematic representation of the cerebello-thalamo-cortical pathway in order to make it easier to localize the seed/target ROIs [6].

1.3 Dentate-rubro-thalamo-cortical (DRTC)

The dentato-rubro-thalamic tract is classically described as a decussating pathway, ascending to the contralateral thalamus. However, recent works applying deterministic fiber tractography in healthy subjects and human brain microdissection have shown the existence of a non-decussating pathway [9].

It originates in the dentate nucleus of the cerebellum, ascends through the brain stem, where the majority of its constituent axons cross the midline at the superior cerebellar decussation (SCP) to synapse with the contralateral red nucleus (RN) in the midbrain, see Fig. 19 [10]. From there, the DRTT continues to the ventrolateral (VL) and ventromedial (VM) nuclei of the thalamus. Technically, the DRTT terminates in the thalamus; however, for functional completeness, in [10] they extended its trajectory to terminate in the primary motor cortex. Whilst an ipsilateral component of the DRTT has been described in the literature, for the current purpose, they have limited the reconstruction to the classical/contralateral DRTT [10].

The main GM constituents of DRTC are the red and dentate nuclei. Thus, to reconstruct DRTC (see Fig. 4, 5, and 6) [11], the DWI non-diffusion b0 image was used for delineating the structures of dentate and red nuclei [11].

DRTC (see Fig. 6) [12] is traditionally described as the only feed-forward cerebellar tract passing from the cerebellar nuclei and dentate nucleus, arriving at the superior cerebellar peduncle, red nucleus, thalamus, and finally terminating at the cerebral cortex. Previous studies referred almost exclusively to contralateral connections, disregarding ipsilateral ones [12].

- ROIs

  The first ROI is seeded in the dentate nucleus, which can be identified at the level of the pontomedullary junction, and the second ROI is in the ipsilateral red nucleus axially at the level of the cerebral peduncle in the pons, see Figs. 2F, 2G, 3C and 3D [11].

  In Karavasilis et al., the first ROI was placed in the dentate nucleus, which was defined at the level of the pontomedullary junction, whereas the second ROI was placed in the red nucleus axially at the level of the cerebral peduncle in the pons. Both ROIs for the DRTC were placed in a b0 DWI image, see supplementary data Fig. 2 [12].

1.4 Fronto-ponto cerebellar tract (FPC)

Karavasilis et al. reconstructed the FPC seen in Fig. 2 [12]. The cerebro-cerebellar loop includes inputs from frontal, prefrontal, orbitofrontal, premotor, and motor cortices. These fibers converge into the pontine nuclei and reach the cerebro-cerebellum cortex, passing through the contralateral MCP as seen in Fig. 3 [9].

Another reconstructed FPC tract can be seen in Fig. 4C, 5A, and 6C [11].

Volumetric segmentation of fronto-cerebellar tracts originating from the left frontal lobe targeting the cerebellum, with more distinct involvement of the right cerebellar hemisphere seen in Fig. 2 [13].

It is noteworthy to mention that recent tractography studies of human brainstem pathways [14] show the fronto-pontine and temporo-parieto-occipito-pontine projections into pontine nuclei, but not their terminations. Their results are unclear as to the dorsal/ventral locations of the two groups of tracts, but both studies are consistent with Karbasforoushan et al. results in suggesting a slightly more rostral termination of the fronto-pontine tract as compared with the temporo-parieto-occipito-pontine axons [15].

The FPC tract that Kamali et al. defined arises from the orbitofrontal and prefrontal cortical areas (the frontal areas anterior to the precentral sulcus). The FPC fibers descend through the ALIC, genu, and the anterior one-third portion of the posterior limb of the internal capsule (PLIC). The FPC fibers continue through the ventro-medial part of the cerebral peduncle caudally to the level of the pons, where they decussate and travel through the contralateral middle cerebellar peduncle (MCP) into the cerebellum [16].

- ROIs

  Keser et al. used a brute force and multiple regions-of-interest (ROIS) tracking method and the Fiber Assignment by Continuous Tracking (FACT) algorithm to reconstruct pathways with an FA threshold of 0.15 and an angle threshold of 70^{o}. The first ROI was placed in MCP, which can be identified at the coronal section of the dorsal surface of brainstem in Red-Green-Blue color map seen in Figs. 2A and 3E [11]. The second ROI was placed in the contralateral frontal lobe, seen in Fig 3F [11], which can be defined as anterior to the central sulcus at the axial level right above cingulate gyrus at the color-coded map [11].

Karavasilis et al. reconstructed the FPC using ROIs 1 and 2 observed in supplementary data Fig. 1 [12].

1.5 Parieto-ponto-cerebellar (PPC)

Karavasilis et al. examined and reconstructed contralateral and ipsilateral connections between the cerebellum and the cerebral lobes (i.e., FPC, TPC, PPC, OPC). Nevertheless, post-mortem histopathological and in vivo DTI studies mainly refer to the presence of contralateral connections in cortico-ponto-cellebelar tracts we can observe in Fig. 3 [12], a tractography reconstruction of the PPC [12].

Using fMRI has allowed to better characterize the cerebellar language-specific activations associated with both expressive and receptive tasks (especially at the level of lobule VI, crus I/II, and midline lobule VII of the right cerebellum), and defined the crossed anatomic interaction with the language association areas within the dominant frontal, parietal, and temporal regions [9].

Identified changes in brain functional activity included the left inferior frontal gyrus (IFG) and the right superior cerebellar lobule VI/crus I (the fronto-cerebellar loop) as well as the left inferior parietal sulcus and the right inferior cerebellar lobule VIIb/VIIIa (the parieto-cerebellar loop) [17].

Prefrontal, sensorimotor, and occipital cortices have connectivity to the medial pontine nuclei, whereas the posterior parietal cortex and temporal lobe strongly correlate with lateral pontine nuclei. Posterior parietal has strong connectivity to the ipsilateral superior lateral pontine nuclei [15]. The posterior parietal cortex tends to have more connections to the superior lateral pons. We also found the posterior parietal cortex and temporal lobe to be correlated with lateral pontine nuclei [15]. We can observe a reconstruction of the aforementioned tracts in Figs. 4B and 4C [18].

The PPC fibers that we define originate from the cortical areas posterior to the precentral sulcus and anterior to the parieto-occipital sulcus, including premotor, primary motor (precentral gyrus), primary sensory (postcentral gyrus), and posterior parietal cortices. The PPC fibers descend side by side with the CST in the centrum semiovale, and then within the posterior two-thirds portion of the PLIC and the most anterior portion of the retrolenticular portion of the internal capsule. These fibers pass through the lateral segment of the middle portion of the cerebral peduncle laterally to the CST or medially to the CST and descend to the basis pontis, where they cross through the latero-lateral fibers. We assigned two different colors in a 3D reconstruction view for the pre-motor and the primary motor portion and parietal portion just to show that by moving from the anterior to the posterior areas, these fibers descend to the lower level of the anterior pontis. Hence, even the most forward parietal fibers cross at a higher level of the basis pontis than the posterior parietal fibers, which cross at the lower levels [16].

We can observe in Fig. 4D [11] a reconstruction of the PPC tract performed to understand the interplay between cerebellar pathways and cerebral macrostructure [11].

- ROIs

  The first ROI was placed in the middle cerebellar peduncle, which was defined at the coronal plane of the dorsal surface of the brainstem in Red-Green-Blue (RGB) color map. The second ROI was different for each cortico-ponto-cerebellar tract. b) for the PPC, the second ROI was placed in the parietal lobe, which was defined as the region posterior to the central sulcus at the axial plane just above the cingulated gyrus in the RGB color map as seen in supplementary data Fig. 1 [12].

  ROI locations (ROI 1 and 2) used for reconstructions of the parieto ponto cerebellar tract seen in Fig. 1 B [16].

The first ROI was placed in MCP, which can be identified at the coronal section of the dorsal surface of the brainstem in the Red-Green-Blue color map seen in supplementary Fig. 1A [12], and the second ROI seen in supplementary Fig. 2B [12]. For PPC, the second ROI observed in supplementary Fig. 3G [12] was placed in the contralateral parietal lobe, which can be identified as the area posterior to the central sulcus at the same level as FPC [11].

1.6 Occipito-ponto-cerebellar tract (OPC)

See Fig. 4 [12], where tracts were found more ipsilateral than contralateral [12]. The cerebellum receives input from the cerebrum via afferent pathways arising from the frontal, parietal, temporal, and occipital cortices relayed through the pontine nuclei [19].

We can observe another reconstruction in Fig. 4E and 5E [11].

This pathway originates from the occipital cortex posterior to the parieto-occipital sulcus, seen in Fig. 3C [16]. While descending through the most posterior portion of the PLIC and through the retrolenticular part of the internal capsule, these fibers continue their course caudally through the dorsolateral portion of the crus cerebri, surrounded by the CST ventrally and by the TPC dorsally. The OPC fibers keep this position all the way down to the basis pontis, where they cross to the other side of the pons and go through the contralateral MCP into the cerebellum [16].

- ROIs

  For [12], they use as ROIs the MCP and the occipital lobe (see Fig. supplementary Fig. 1A and 1B) [12].

1.7 Olivocerebellar tract (OVC)

The collaterals to the dentate nucleus constitute a reciprocal loop connecting the inferior olivary nucleus with the deep cerebellar nuclei (olivary-dentate-olivary loop,

Fig. 1B [8]. Fiber solutions that do not connect to the dentate nucleus reach the cerebellar cortex (olivary-cerebellar cortex connections, Fig. 1B-I) [8], crossing at right angles with fibers in the cortex that have a location and orientation consistent with parallel fibers [8].

This pathway consists of axonal projections originating from the inferior olive (IO) and terminating in the cerebellar cortex. From their origin, these fibers run medially to cross over at the midsagittal plane, passing either through or above the contralateral inferior olive. They then reach the medullary white matter beneath the lateral surface, eventually integrating into the inferior cerebellar peduncle (ICP) [20, 21].

The inferior olivary nucleus (ION) was set as the seed point, and the contralateral cerebellum was set as a terminate region instead of the contralateral cerebellar cortex because the climbing fibers usually sprout collateral branches before reaching the cerebellar cortex; the pontine was defined as a region of avoidance (ROA) to ensure that fibers originating from the ION passed through the contralateral inferior cerebellar peduncle (ICP) and finally ended at the contralateral cerebellum; a horizontal plane right upon the ION was additionally set as an ROA to rule out longitudinal fibers, and another 2 horizontal planes upon the pontine and a vertical plane in the posterior part of the pontine were set as ROAs (Fig. 2) [22] the RN and unilateral cerebellum were loaded from the built-in region list in the DSI studio; the pontine was drawn to cover all pontine nucleus regions, and the ION was drawn on both sides separated by the middle line in the fusiform [22].

The results of both olivocerebellar tracts failed to reflect the anatomical facts in almost every participant. We tried to interpret the result from several aspects. First, the olivocerebellar tracts originate from the ION, traveling first across the midline and finally joining the contralateral ICP before entering the cerebellum, thus forming cross fibers in this region. The olivocerebellar tracts pass through the restiform body, where the spinocerebellar tract is located, with both running laterally to the trigeminal nerve

branches to enter the ICP. It is difficult to separate the olivocerebellar tracts due to the parallel fibers and complex adjacent relationships. Furthermore, the brainstem, especially the pontine, has several disadvantages for fiber tracking: a small volume, complex fiber-crossing situations, and motion artefacts [22].

- ROIs

  Tracking from this ROI (inferior olivary nucleus), we identified a pathway entering the cerebellum through the ICP and connecting to: 1) the dentate nucleus (light green, Fig. 1A) and 2) [8] the cerebellar cortex (dark green, Fig. 1A) [8]. This pathway is consistent with the trajectory of the olivocerebellar climbing fiber system [8].

1.8 Periaqueductal gray cerebellar tract (PAG)

The streamlines arising from the PAG ran through the superior cerebellar peduncle and follow the arbor vitae of the cerebellum, reaching nuclei, vermal regions, and lobules. Connectivity patterns joining the PAG, respectively, with the deep cerebellar nuclei (Fig. 1) [23], the entire vermis (Fig. 3) [23], and lobules (Fig. 4) [23] have been successfully reconstructed [23].

The periaqueductal gray matter (PAG) is a midbrain structure situated at the confluence of ascending sensory and descending higher center pathways. The PAG plays an essential role in the integration of these inputs [24].

- ROIs

  The ROI of the PAG was obtained from the Keuken and Forstmann's 7T atlas that provides ROIs obtained from high-resolution MP2RAGE and FLASH scans warped in MNI space [25]. In [26], they used the periaqueductal grey (PAG; mask adapted from [27]), seen in Figs. 5A and 6 [26].

1.9 Spinocerebellar tract (SPNC)

The dorsal spinocerebellar tract ascending in the laterodorsal medulla oblongata and terminating in the vermis and paravermis of the anterior lobe. The dorsal spinocerebellar tract appears flattened at the level of the restiform corpus, runs within the cerebellum inside the MCP, and outside the SCP in the upper cerebellum, and fans preferentially to the vermian part of lobules I–V [4].

SPNC pathways mainly originate from the spinal cord and pass through the ICP to enter the cerebellum, see Figs. 4A and 5A [11].

The spino-cerebellar loop passes through the somatosensory cortex, visual and auditory receptors, the spinal cord, through the dorsal and ventral spino-cerebellar tracts. The spino-cerebellum corresponds to the intermediate compartment, including the paravermis and the interposed nucleus (including the globose and emboliform nuclei), and the medial compartment, which involves the vermis and the fastigial nucleus (see Fig. 3) [9].

- ROIs

  For the spinocerebellar tract, first, the ROI is seeded in ICP, which is located at the upper medulla level of the brain (see Fig. 3A) [11] and the second ROI is seeded at the ipsilateral cerebellar hemisphere at the same axial slice (see Fig. 3B) [11].

1.10 Inferior cerebellar peduncle (ICP)

The ICP consists mainly of afferent sensory fibers projecting from the spinal cord to the cerebellum, and in [10], they reconstructed it as a single lateralized bundle using the dentate, fastigial, and interposed nuclei of the cerebellum, and the ipsilateral medulla oblongata, see Figs. 19D and 19G [10].

In Fig. 2 [28], red identifies the cortico-spinal tract, blue the SCP, green the MCP, and yellow the ICP pathways [28].

The ICP (or corpus restiforme), which has a cylindrical aspect at the level of the medulla, flattens at the level of the inferior part of the fourth ventricle and is squeezed between the superior and middle cerebellar peduncles before its fibers fan out toward the anterior vermis and lobules, see Fig.3 [29]. More ICP fibers entered the anterior lobules (lobule I–V, anterior to the primary fissure) (black arrowheads), compared to the posterior lobules (lobule VI to VIII; posterior to the primary fissure) (white arrowheads) [29].

- ROIs

  For the IPC in Takahashi et al., the posterior pons and cerebellar hemisphere were used as ROIs [28].

  In [29], the seed region was chosen in the ipsilateral restiform body (Fig. 1C [29], top, green ROI). The non-linear 1 mm Probabilistic Atlas of the Cerebellum was chosen as a waypoint as well as a stop region, and the posterior fossa midline was chosen as an exclusion mask. Finally, to prevent streamlines from entering the cerebellum directly from the restiform body by crossing the cerebello-medullary fissure, an exclusion mask covering the tonsils was used, as seen in Fig. 1C. [29].

1.11 Middle cerebellar peduncle (MCP)

The MCPs are large paired bundles that connect the brainstem to the cerebellum on both sides. They are often reconstructed in neuroimaging studies as a single commissural bundle connecting both cerebellar hemispheres. In [10] they reconstructed the MCP as a whole for each side using the contra-lateral pons and cerebellar cortex. The resulting streamlines cross the midline in the pons, in line with its neuroanatomical definition, see Figs. 19E and 19H [10].

The majority of fibers from the MCP (or brachium pontis) run to the posterior rather than anterior lobules (Fig. 3) [29], and the MCP, which is the largest of the peduncles, had the most streamlines per voxel [29].

The MCP traverses laterally toward the trigeminal nerve as the transverse pontine fibers pass laterally in relation to the cerebellopontine fissure. The MCP extends from the pons to the cerebellum posteriorly and medially to spread over all the cerebellum except the nodulus and flocculus. The intracerebellar spread of the MCP fibers covers the DN, see Fig. 5D [30].

- ROIs

  For the MCP in [28], the ROIs used were the anterior pons and cerebellar hemisphere.

  In [29], the seed region was chosen in the ipsilateral pons. An exclusion mask in the midline of the posterior fossa was used to prevent streamlines from crossing to the contralateral side, either through the pons or through the cerebellar cortex, which is continuous through both hemispheres (Fig. 1B) [29].

1.12 Superior cerebellar peduncle (SCP)

Streamlines from the SCP may be erroneously tracked into the adjacent central tegmental tract or medial longitudinal fasciculus. However, the majority of these aberrant tracts do only appear at low probabilities. Their investigation Van et al,. showed a slightly more lateral position of the SCP in the roof of the fourth ventricle. Further, the parcellations extend further into the cerebellar hemispheres as well as the mesencephalon and clearly demonstrate the decussation of the SCPs.

In Fig. 4 [30], the SCP originates from the dentate, globus, and emboliform nuclei; the fibers of the SCP decussate dorsally and rostrally to the interpeduncular nucleus before extending to the nucleus ruber to reach the ventrolateral thalamus [30]. The congregated SCP segment reached the lateral edge of the upper half of the fourth ventricle, where it was renamed as the ventricular segment en route to its junction with the lateral lemniscus along the cerebello mesencephalic fissure. The ventricular segment formed the lateral component of the upper part of the fourth ventricular roof,

and, at this level, the SCPs on both sides were related to the superior medullary velum medially. It should be recalled that the dorsal part of the upper third of the ventricular segment of the SCP was situated within the boundaries of the cerebello mesencephalic fissure in the quadrigeminal cistern. As the SCP fibers climbed and approached their junction with the tectum, the ventricular segment submerged deep into the inferior colliculus to become the distal intramesencephalic segment. The decussation of the SCP was located at the pontomesencephalic junction, ventral to the inferior colliculus and the aqueduct [4, 30].

- ROIs

  For the SCP in [28] the ROI was the posterior pons and deep cerebellar white matter. In [29], the seed region was chosen in the ipsilateral dentate nucleus. The contralateral thalamus, as well as the stop region (i.e., streamlines had to go through the thalamus to be considered valid, and they were terminated upon entering the thalamus), see Fig. 1A [29].

2 Atlas tract reconstruction

The cerebellar pathways included in the atlas are presented in Figs. 1 and 2. Figure 1 shows the 12 cerebellar connections that compose the atlas, with each bilateral connection displayed as a single combined panel. Figure 2 shows the same pathways at the fascicle level: the 8 bilateral connections are split into their left and right components which, together with the 4 unpaired tracts (MCP, OVC, PAG, and SCP), yield the 20 fascicles of the atlas, shown here in coronal and sagittal views

3 Atlas validation on a different group

Fig. 3 represents the results for the automatic segmentation for one test subject with the three different tracking thresholds (0.04, 0.08, and 0.12) and for the two optimal segmentation distance thresholds (DT1 and DT2).

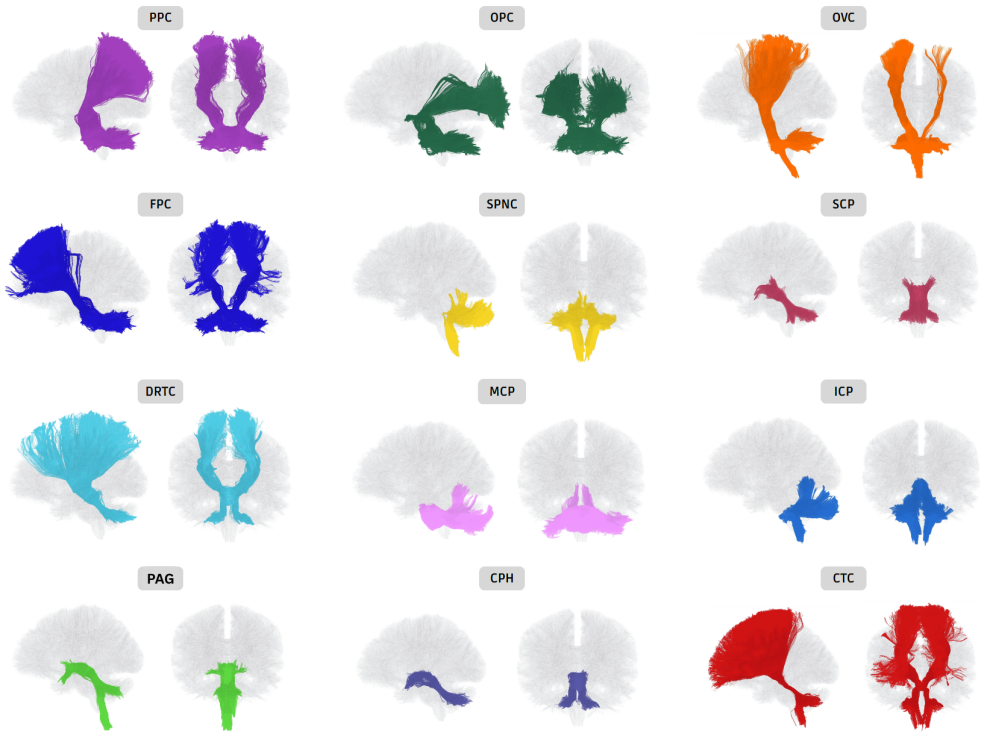

Fig. 1: The 12 cerebellar connections included in the atlas (bilateral tracts shown combined), in coronal and sagittal views.

Fig. 4 shows the automatic segmentation for the periaqueductal grey cerebellar (PAG) tract using the tracking threshold of 0.08 and using the second optimal segmentation distance thresholds (DT2).

Figs. 5 and 6 show the 3 cerebellar peduncles using manual and automatic segmentation, respectively. For automatic segmentation, the tracking threshold is 0.08, and the first optimal segmentation distance threshold (DT1) was employed.

Fig. 7 shows a visual comparison of the manual, automatic, and atlas segmentation of all 20 tracts for a test subject. Also, Fig. 8 shows the lowest dice for this same test subject, belonging to the CPH_R, CTC_R, DRTC_R, and FPC_R.

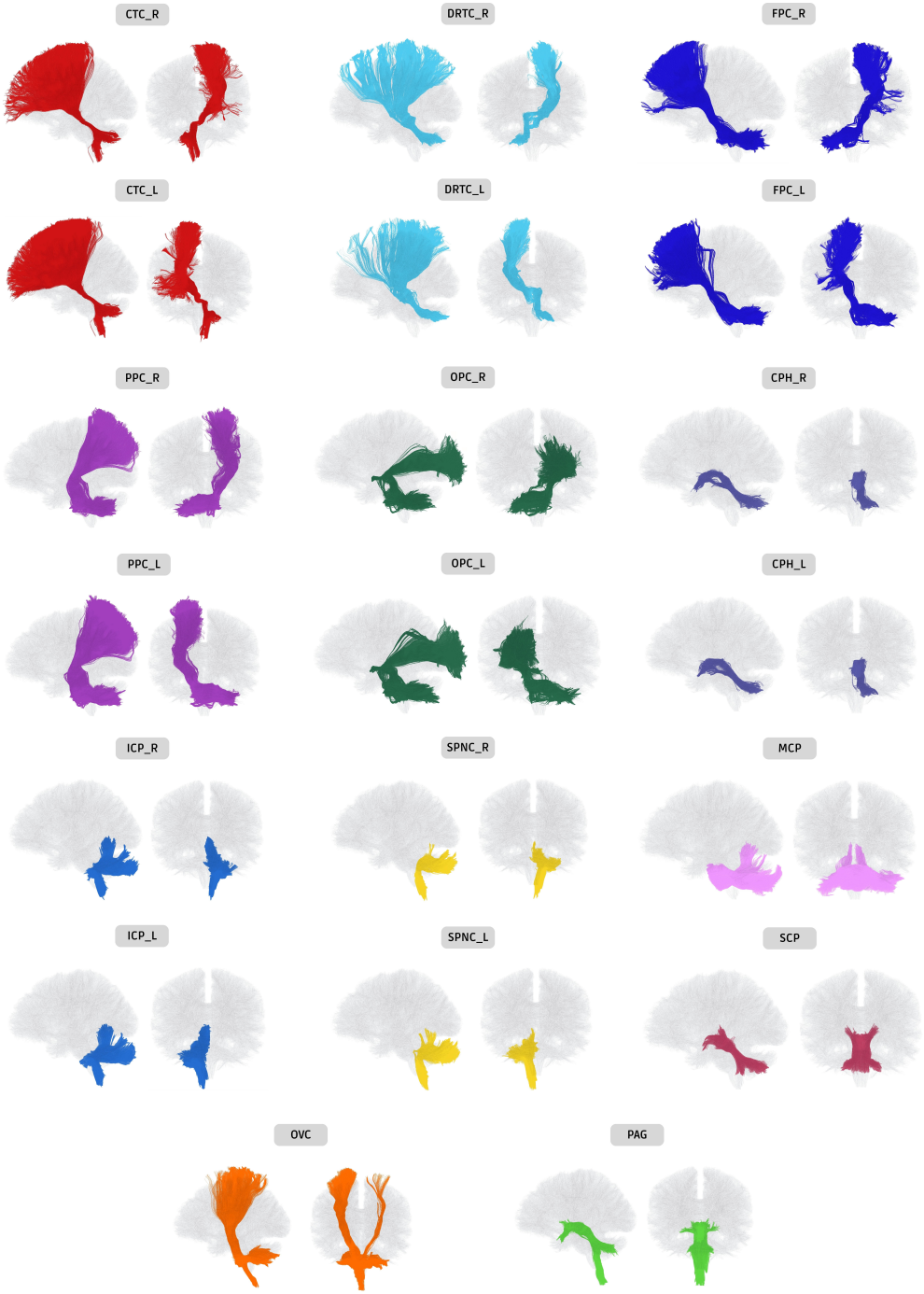

Fig. 2: The 20 cerebellar fascicles of the atlas (bilateral tracts shown separately as left/right) in coronal and sagittal views.

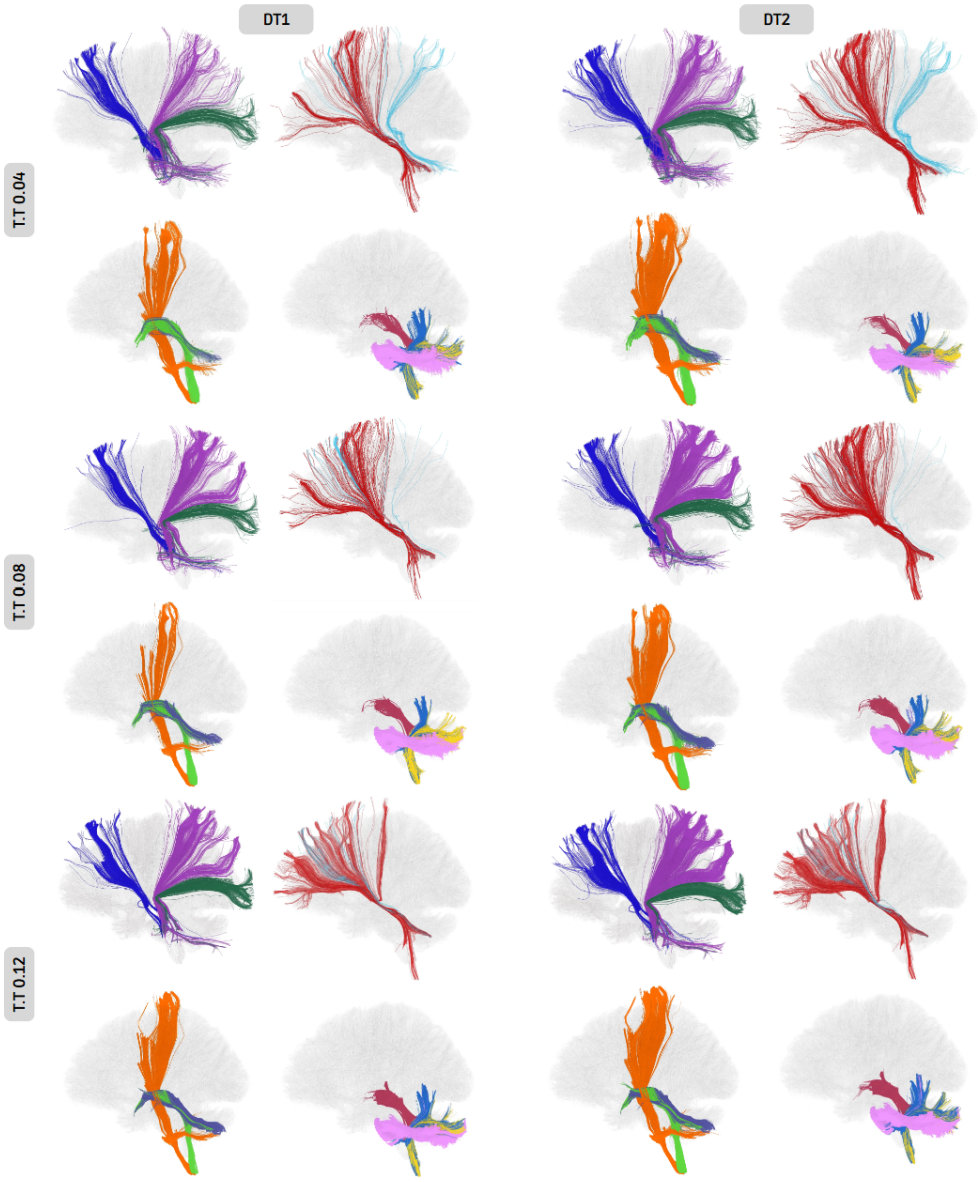

Fig. 3: Automatic segmentation of all 20 cerebellar fascicles for a single validation subject (117021), shown for the three whole-brain tracking thresholds (T.T): 0.04, 0.08, and 0.12, and the two optimal segmentation distance thresholds (DT1 and DT2).

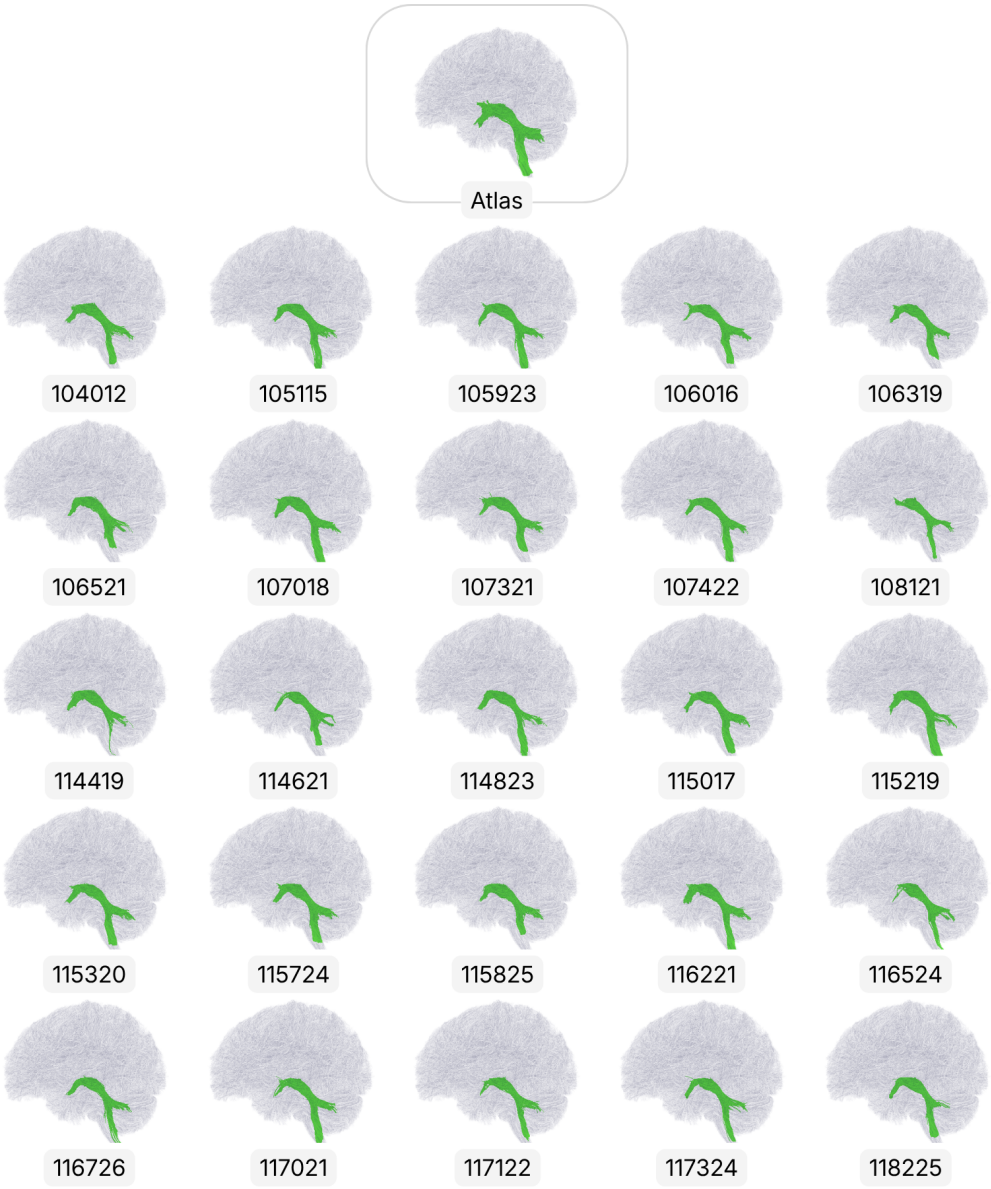

Fig. 4: Automatic tractography reconstruction for the PAG tract for the 25 subjects using the tracking threshold 0.08 and DT2.

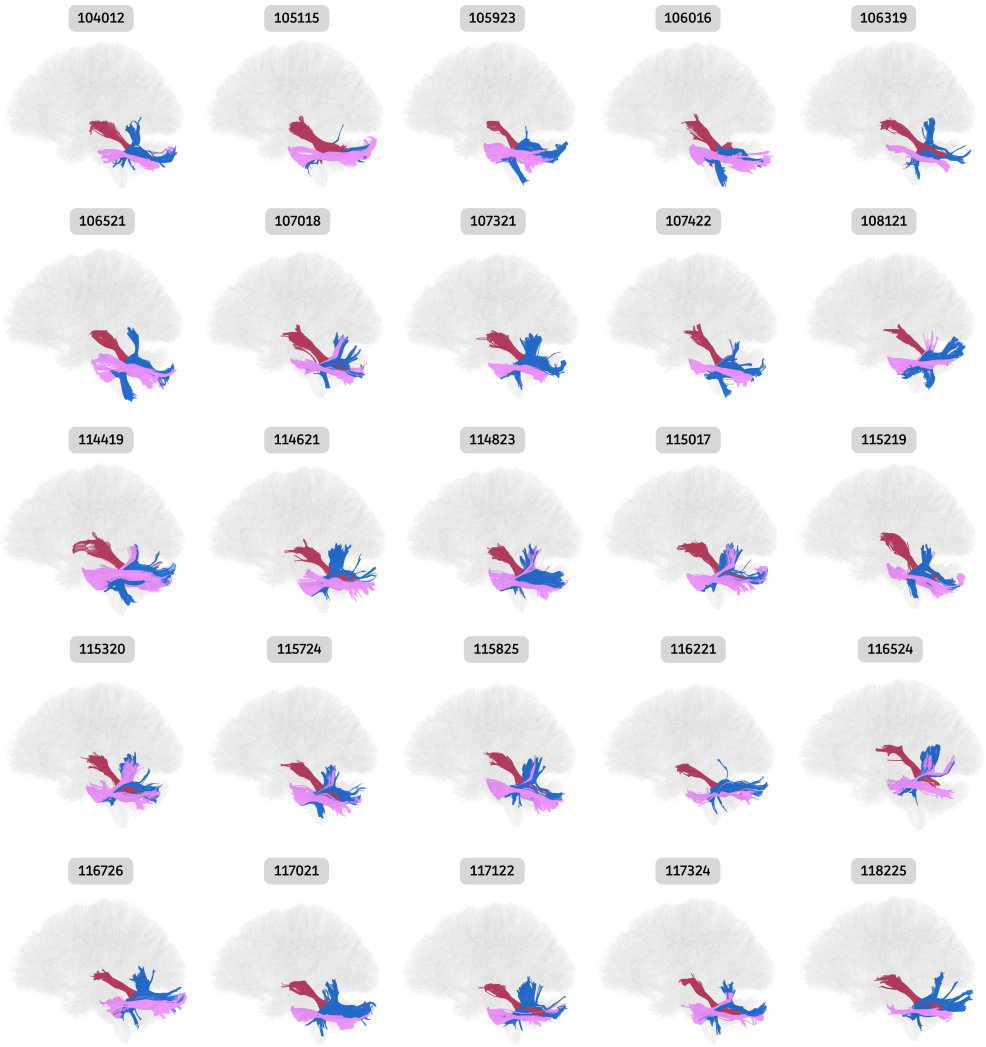

Fig. 5: Manual segmentation for the 25 subjects of the 3 cerebellar peduncles (MCP, ICP, and SCP), as seen in sagittal view.

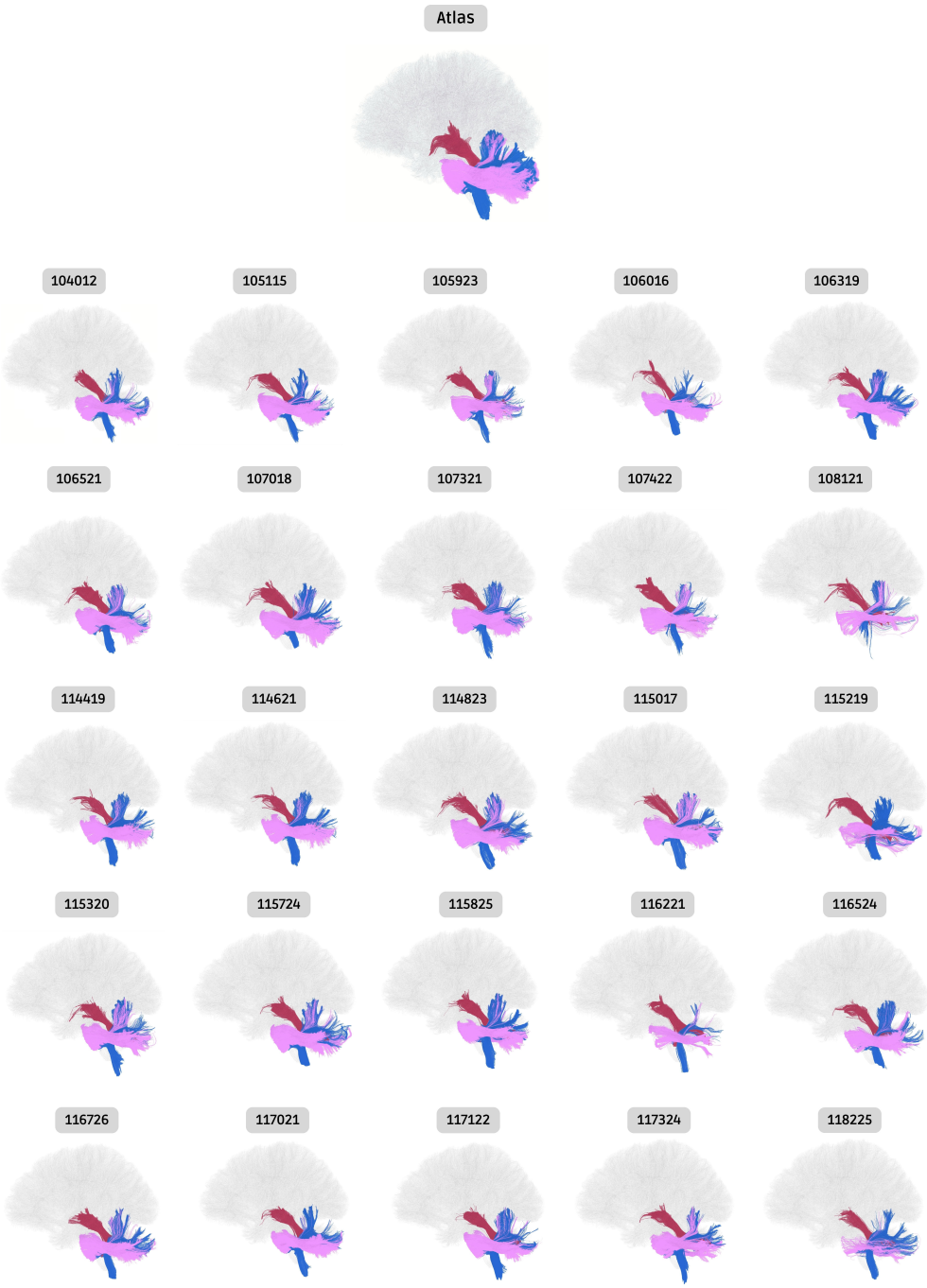

Fig. 6: Automatic segmentation for the 25 subjects of the 3 cerebellar peduncles (MCP, ICP, and SCP) with a tracking threshold of 0.08 and DT1, seen in sagittal view.

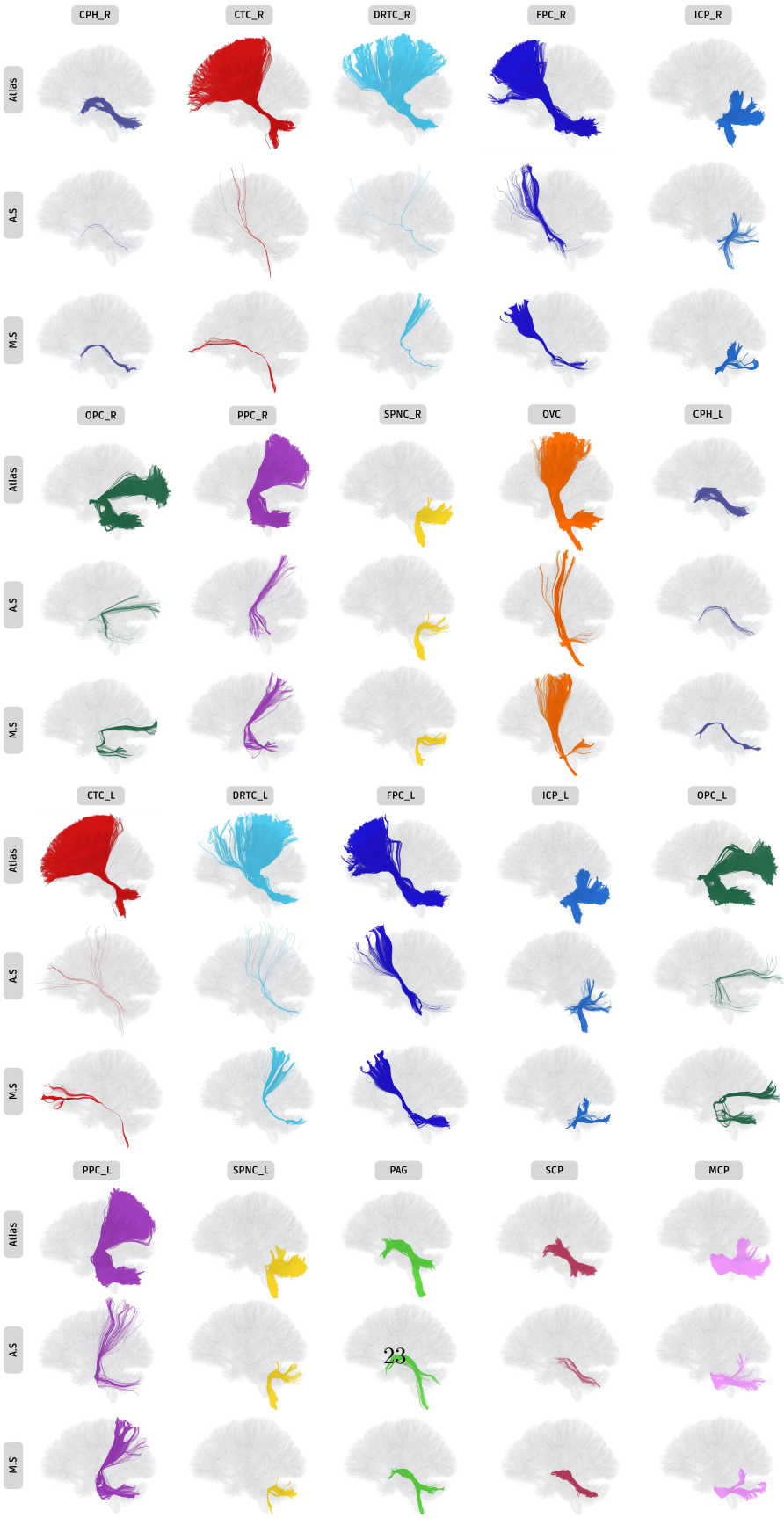

Fig. 7: Visual comparison of the atlas, automatic, and manual segmentation of all 20 cerebellar fascicles for a validation subject (115017). For each fascicle, three rows are shown: the atlas reference tract (Atlas), the automatic segmentation (A.S), and the manual segmentation (M.S).

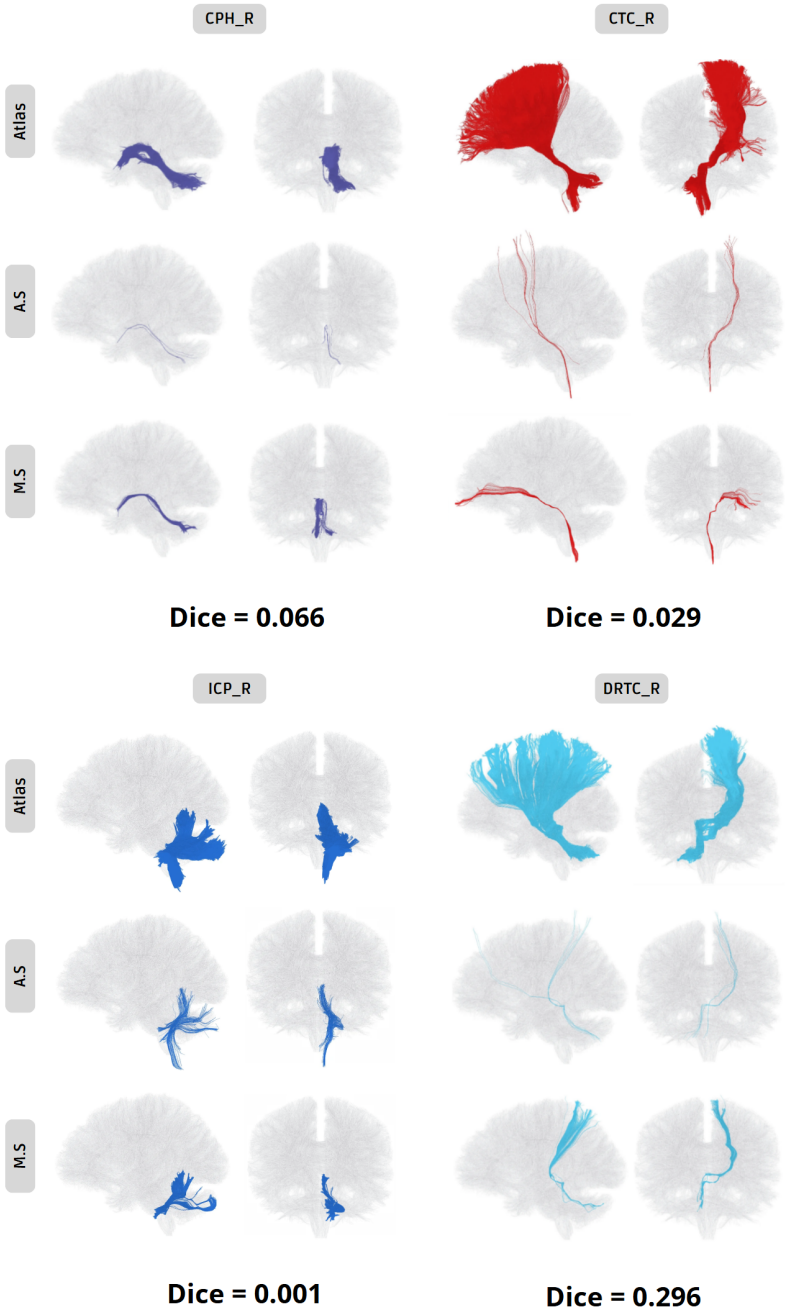

Fig. 8: The four fascicles with the lowest Dice coefficient for validation subject 115017 (CPH_R, CTC_R, DRTC_R, and FPC_R). For each fascicle, three rows are shown: the atlas reference tract (Atlas), the automatic segmentation (A.S), and the manual segmentation (M.S). Also, the corresponding Dice coefficient is reported beneath each fascicle.

References

[1] Kamali, A., Karbasian, N., Rabiei, P., Cano, A., Riascos, R.F., Tandon, N., Arevalo, O., Ocasio, L., Younes, K., Khayat-khoei, M., Mirbagheri, S., Hasan, K.M.: Revealing the cerebello-ponto-hypothalamic pathway in the human brain. Neuroscience Letters **677**, 1–5 (2018)

[2] Çavdar, S., Esen Aydın, A., Algin, O., Aydoğmuş, E.: Fiber dissection and 3-tesla diffusion tensor tractography of the superior cerebellar peduncle in the human brain: emphasize on the cerebello-hypthalamic fibers. Brain Structure and Function **225**, 121–128 (2020)

[3] Palesi, F., De Rinaldis, A., Castellazzi, G., Calamante, F., Muhlert, N., Chard, D., Tournier, J.D., Magenes, G., D'Angelo, E., Gandini Wheeler-Kingshott, C.A.: Contralateral cortico-ponto-cerebellar pathways reconstruction in humans in vivo: implications for reciprocal cerebro-cerebellar structural connectivity in motor and non-motor areas. Scientific Reports **7**(1), 12841 (2017)

[4] Habas, C., Manto, M.: Probing the neuroanatomy of the cerebellum using tractography. Handbook of Clinical Neurology **154**, 235–249 (2018)

[5] Palesi, F., Tournier, J.-D., Calamante, F., Muhlert, N., Castellazzi, G., Chard, D., D'Angelo, E., Wheeler-Kingshott, C.A.: Contralateral cerebello-thalamo-cortical pathways with prominent involvement of associative areas in humans in vivo. Brain Structure and Function **220**, 3369–3384 (2015)

[6] Palesi, F., Tournier, J.-D., Calamante, F., Muhlert, N., Castellazzi, G., Chard, D., D'Angelo, E., Wheeler-Kingshott, C.G.: Reconstructing contralateral fiber tracts: methodological aspects of cerebello-thalamocortical pathway reconstruction. Functional Neurology **31**(2), 1–10 (2015)

[7] Calamante, F., Tournier, J.-D., Jackson, G.D., Connelly, A.: Track-density imaging (tdi): super-resolution white matter imaging using whole-brain track-density mapping. NeuroImage **53**(4), 1233–1243 (2010)

[8] Granziera, C., Schmahmann, J.D., Hadjikhani, N., Meyer, H., Meuli, R., Wedeen, V., Krueger, G.: Diffusion spectrum imaging shows the structural basis of functional cerebellar circuits in the human cerebellum in vivo. PLOS One **4**(4), 5101 (2009)

[9] De Benedictis, A., Rossi-Espagnet, M.C., Palma, L., Carai, A., Marras, C.E.: Networking of the human cerebellum: From anatomo-functional development to neurosurgical implications. Frontiers in Neurology **13**, 806298 (2022)

[10] Radwan, A.M., Sunaert, S., Schilling, K., Descoteaux, M., Landman, B.A., Vandenbulcke, M., Theys, T., Dupont, P., Emsell, L.: An atlas of white matter anatomy, its variability, and reproducibility based on constrained spherical deconvolution of diffusion mri. NeuroImage **254**, 119029 (2022)

[11] Keser, Z., Hasan, K.M., Mwangi, B.I., Kamali, A., Ucisik-Keser, F.E., Riascos, R.F., Yozbatiran, N., Francisco, G.E., Narayana, P.A.: Diffusion tensor imaging of the human cerebellar pathways and their interplay with cerebral macrostructure. Frontiers in Neuroanatomy **9**, 41 (2015)

[12] Karavasilis, E., Christidi, F., Velonakis, G., Giavri, Z., Kelekis, N.L., Efstathopoulos, E.P., Evdokimidis, I., Dellatolas, G.: Ipsilateral and contralateral cerebro-cerebellar white matter connections: a diffusion tensor imaging study in healthy adults. Journal of Neuroradiology **46**(1), 52–60 (2019)

[13] Soelva, V., Hernáiz Driever, P., Abbushi, A., Rueckriegel, S., Bruhn, H., Eisner, W., Thomale, U.-W.: Fronto-cerebellar fiber tractography in pediatric patients

following posterior fossa tumor surgery. Child's Nervous System **29**, 597–607 (2013)

[14] Tang, Y., Sun, W., Toga, A.W., Ringman, J.M., Shi, Y.: A probabilistic atlas of human brainstem pathways based on connectome imaging data. Neuroimage **169**, 227–239 (2018)

[15] Karbasforoushan, H., Tian, R., Baker, J.: There is a topographic organization in human cortico-pontine connectivity. Brain Communications **4**(2), 047 (2022)

[16] Kamali, A., Kramer, L.A., Frye, R.E., Butler, I.J., Hasan, K.M.: Diffusion tensor tractography of the human brain cortico-ponto-cerebellar pathways: a quantitative preliminary study. Journal of Magnetic Resonance Imaging **32**(4), 809–817 (2010)

[17] Sobczak-Edmans, M., Lo, Y.-C., Hsu, Y.-C., Chen, Y.-J., Kwok, F.Y., Chuang, K.-H., Tseng, W.-Y.I., Chen, S.A.: Cerebro-cerebellar pathways for verbal working memory. Frontiers in Human Neuroscience **12**, 530 (2019)

[18] Meola, A., Yeh, F.-C., Fellows-Mayle, W., Weed, J., Fernandez-Miranda, J.C.: Human connectome-based tractographic atlas of the brainstem connections and surgical approaches. Neurosurgery **79**(3), 437–455 (2016)

[19] Argyropoulos, G.D., Christidi, F., Karavasilis, E., Velonakis, G., Antoniou, A., Bede, P., Seimenis, I., Kelekis, N., Douzenis, A., Papakonstantinou, O., Efstathopoulos, E., Ferentinos, P.: Cerebro-cerebellar white matter connectivity in bipolar disorder and associated polarity subphenotypes. Progress in Neuro-Psychopharmacology and Biological Psychiatry **104**, 110034 (2021)

[20] Sugihara, I., Wu, H.-S., Shinoda, Y.: Morphology of single olivocerebellar axons labeled with biotinylated dextran amine in the rat. Journal of Comparative

Neurology **414**(2), 131–148 (1999)

[21] Luo, Y., Sugihara, I.: The olivocerebellar tract. In: Essentials of Cerebellum and Cerebellar Disorders: A Primer For Graduate Students, pp. 41–45. Springer, ??? (2023)

[22] Yin, H., Zong, F., Deng, X., Zhang, D., Zhang, Y., Wang, S., Wang, Y., Zhao, J.: The language-related cerebro-cerebellar pathway in humans: a diffusion imaging–based tractographic study. Quantitative Imaging in Medicine and Surgery **13**(3), 1399 (2023)

[23] Cacciola, A., Bertino, S., Basile, G.A., Di Mauro, D., Calamuneri, A., Chillemi, G., Duca, A., Bruschetta, D., Flace, P., Favaloro, A., Calabrò, R.S., Anastasi, G., Milardi, D.: Mapping the structural connectivity between the periaqueductal gray and the cerebellum in humans. Brain Structure and Function **224**(6), 2153–2165 (2019)

[24] Ezra, M., Faull, O.K., Jbabdi, S., Pattinson, K.T.: Connectivity-based segmentation of the periaqueductal gray matter in human with brainstem optimized diffusion mri. Human Brain Mapping **36**(9), 3459–3471 (2015)

[25] Keuken, M.C., Forstmann, B.U.: A probabilistic atlas of the basal ganglia using 7 t mri. Data in brief **4**, 577–582 (2015)

[26] Reisert, M., Weiller, C., Hosp, J.A.: Displaying the autonomic processing network in humans–a global tractography approach. NeuroImage **231**, 117852 (2021)

[27] Edlow, B.L., Takahashi, E., Wu, O., Benner, T., Dai, G., Bu, L., Grant, P.E., Greer, D.M., Greenberg, S.M., Kinney, H.C., Folkerth, R.D.: Neuroanatomic connectivity of the human ascending arousal system critical to consciousness and its disorders. Journal of Neuropathology & Experimental Neurology **71**(6), 531–546

(2012)

[28] Takahashi, E., Song, J.W., Folkerth, R.D., Grant, P.E., Schmahmann, J.D.: Detection of postmortem human cerebellar cortex and white matter pathways using high angular resolution diffusion tractography: a feasibility study. Neuroimage **68**, 105–111 (2013)

[29] Van Baarsen, K., Kleinnijenhuis, M., Jbabdi, S., Sotiropoulos, S.N., Grotenhuis, J., Walsum, A.v.C.: A probabilistic atlas of the cerebellar white matter. NeuroImage **124**, 724–732 (2016)

[30] Baran, O., Baydin, S., Mirkhasilova, M., Bayramli, N., Bilgin, B., Middlebrooks, E., Ozlen, F., Tanriover, N.: Microsurgical anatomy and surgical exposure of the cerebellar peduncles. Neurosurgical Review, 1–23 (2022)